Lewis Kate (Orcid ID: 0000-0003-2909-2570)
Mills Matthew (Orcid ID: 0000-0002-9738-5589)
Selz Virginia (Orcid ID: 0000-0002-1559-3641)

TITLE

Photoacclimation of Arctic Ocean phytoplankton to shifting light and nutrient limitation

RUNNING HEAD

Photoacclimation to shifting light and nutrients

KEYWORDS

photophysiology, photoacclimation, nutrient limitation, light limitation, Arctic, Chukchi Sea, phytoplankton

AUTHORS

Kate M. Lewis[1] kmlewis@stanford.edu (corresponding author)
Alexandra E. Arntsen[2], Alexandra.E.Arntsen.TH@dartmouth.edu
Pierre Coupel[3] Pierre.Coupel@takuvik.ulaval.ca
Hannah Joy-Warren[1] hjoyw@stanford.edu
Kate Lowry[4] klowry@whoi.edu
Atsushi Matsuoka[3] Atsushi.Matsuoka@takuvik.ulaval.ca
Matthew M. Mills[1] mmmills@stanford.edu
Gert L. van Dijken[1] gertvd@stanford.edu
Virginia Selz[1] vselz@stanford.edu
Kevin R. Arrigo[1] arrigo@stanford.edu

[1] Department of Earth System Science, Stanford University, Stanford, CA, 94305.
[2] Thayer School of Engineering, Dartmouth College, Hanover, NH 03755.
[3] Takuvik Joint International Laboratory (CNRS-ULaval), Département de Biologie, Université Laval, Québec, QC, G1V 0A6, Canada.

This is the author manuscript accepted for publication and has undergone full peer review but has not been through the copyediting, typesetting, pagination and proofreading process, which may lead to differences between this version and the Version of Record. Please cite this article as doi: 10.1002/lno.11039

[4] Department of Biology, Woods Hole Oceanographic Institution, Woods Hole, MA 02543.

ABSTRACT

As the physical environment of the Arctic Ocean shifts seasonally from ice-covered to open water, the limiting resource for phytoplankton growth shifts from light to nutrients. To understand the phytoplankton photophysiological responses to these environmental changes, we evaluated photoacclimation strategies of phytoplankton during the low-light, high-nutrient ice-covered spring and the high-light, low-nutrient ice-free summer. Field results show that phytoplankton effectively acclimated to reduced irradiance beneath the sea ice by maximizing light absorption and photosynthetic capacity. In fact, exceptionally high maximum photosynthetic rates and efficiency observed during the spring demonstrate that abundant nutrients enable pre-bloom phytoplankton to become “primed” for increases in irradiance. This ability to quickly exploit increasing irradiance can help explain the ability of phytoplankton to generate massive blooms beneath sea ice. In comparison, phytoplankton growth and photosynthetic rates are reduced post-bloom due to severe nutrient limitation. These results advance our knowledge of photoacclimation by polar phytoplankton in extreme environmental conditions and indicate how phytoplankton may acclimate to future changes in light and nutrient resources under continued climate change.

INTRODUCTION

Each year, the Arctic Ocean (AO) environment undergoes a radical transformation. Dramatic seasonal changes in the physical environment, which impact light and nutrient availability, dictate the timing and magnitude of the annual phytoplankton bloom (Sakshaug 2004; Tremblay and Gagnon 2009; Popova et al. 2012). For instance, changes in snow and sea ice cover dramatically alter the light environment experienced by phytoplankton (Mundy et al. 2005; Frey et al. 2011). In the spring, prior to the phytoplankton bloom, extensive snow and sea ice cover limits the photosynthetically active radiation (PAR, 400-700 nm) that is available for phytoplankton growth to only 2% of incoming irradiance (Sakshaug 2004; Arntsen 2018). As incoming solar irradiance increases, melt ponds form and sea ice retreats, resulting in greater transmission of PAR to the surface ocean, which triggers the seasonal phytoplankton bloom (Sakshaug 2004; Hill et al. 2005; Tremblay and Gagnon 2009; Arrigo et al. 2014). In fact, solar radiation can increase so much that phytoplankton must protect themselves against photodamage (Sakshaug 2004; Leu et al. 2007).

Similar to the seasonal pattern of light, the availability of dissolved nitrate (NO_3^-), the primary limiting nutrient for phytoplankton growth in the AO (Tremblay et al. 2006; Lowry et al. 2015, Danielson et al. 2017), shifts significantly throughout the phytoplankton growing season (Cota et al. 1996; Codispoti et al. 2005, 2009; Tremblay and Gagnon 2009). For example, beneath spring ice-cover in the Chukchi Sea, the water column is weakly stratified with remarkably high pre-bloom NO_3^- concentrations (>8 μM) throughout the shelf (Codispoti et al. 2005, 2009; Arrigo et al. 2017; Lowry et al. 2018). As the phytoplankton bloom develops, NO_3^- in surface waters becomes increasingly depleted due to assimilation into N-containing macromolecules (Hansell et al. 1993; Codispoti et al. 2005, 2009; Hill and Cota 2005; Varela et

al. 2013; Lowry et al. 2015; Danielson et al. 2017). Just prior to the peak of the bloom, phytoplankton have ample light and nutrients and achieve their maximum growth rates (Arrigo et al. 2014). By the end of the bloom in summer, phytoplankton consumption completely depletes surface NO_3^-, leaving a largely inaccessible NO_3^- reservoir beneath a strongly stratified mixed layer, resulting in a high-light, low-nutrient (HLLN) post-bloom environment (Cooper et al. 1997; Codispoti et al. 2005, 2009; Lowry et al. 2015; Danielson et al. 2017).

Thus, the pre-bloom springtime conditions represent a low-light, high-nutrient (LLHN) environment where light limits the initiation of phytoplankton growth (Hill et al. 2005; Tremblay and Gagnon 2009). While the initiation of the bloom is controlled by light availability (Hill et al. 2005; Arrigo et al. 2017; Lowry et al. 2018), the NO_3^- inventory controls the overall magnitude of the bloom (Walsh et al. 2005; Tremblay and Gagnon 2009). Thus, the limiting resource for phytoplankton growth shifts from light in spring to nutrients in summer.

In order to photoacclimate during the seasonal transition from light to nutrient limitation, phytoplankton must adjust their photosynthetic machinery. In response to changing irradiance, phytoplankton modify their pigment composition, thereby altering light absorption and protecting against photoinhibition (Eberhard et al. 2008; Kropuenske et al. 2009; Nymark et al. 2009). Phytoplankton may also adjust the number and size of their photosynthetic units depending on available light energy (Kolber et al. 1988b; Falkowski and Raven 2007). These changes in pigments and photosynthetic machinery affect measurable photosynthetic parameters. For example, in low light, by increasing the size of their photosynthetic units, phytoplankton may increase functional absorption cross-section (σ_{PSII}) and photosynthetic efficiency (α^*), thereby lowering the photoacclimation parameter (E_k) to match ambient light levels (Falkowski and Owen 1980; Moore et al. 2006). Alternatively, phytoplankton can increase the number of

photosynthetic units, which increases cellular absorption of light without changing σ_{PSII} (Moore et al. 2006). As light increases, phytoplankton respond by increasing photosynthetic proteins related to both the light reactions and carbon fixation, thereby elevating maximum photosynthetic rates (P^*_{max}) (Eberhard et al. 2008; Nymark et al. 2009). If light levels reach damaging intensities, phytoplankton typically replace photosynthetic pigments with photoprotective pigments to minimize photoinhibition and consequently diminish quantum yield of photosynthesis (Φ_m) (Kiefer and Mitchell 1983; Falkowski et al. 1985; Babin et al. 1996). However, because synthesizing proteins and pigments requires nutrients (Geider et al. 1993; Eberhard et al. 2008), NO_3^- limitation can impede these photoacclimation responses by restricting growth, quantum yield and photochemical efficiency of photosystem II (Geider et al. 1993; van de Poll et al. 2005), while increasing susceptibility to photoinhibition (Kiefer 1973; Litchman et al. 2002).

While the dynamics of the annual marginal sea ice zone bloom have been well documented in the Chukchi Sea (Tremblay et al. 2006; Brown et al. 2015; Danielson et al. 2017), there is a scarcity of physiological data for phytoplankton beneath the ice prior to the spring bloom. Expansive sea ice cover and inhospitable conditions have historically deterred field sampling of the sea ice zone in the spring. Moreover, because sea ice and snow reflect and attenuate light (Grenfell and Maykut 1977; Perovich and Polashenski 2012), the conventional wisdom has been that phytoplankton production is restricted to waters free of sea ice. Consequently, field surveys of the AO are severely biased towards the summer months (Matrai et al. 2013). However, the discovery of a massive under-ice bloom, with biomass reaching > 1290 mg Chl *a* m^{-2} and net primary production (NPP) rates as high as 3.7 g C m^{-2} d^{-1}, altered the established scientific narrative regarding the progression of phytoplankton blooms in the AO.

The presence of this huge under-ice bloom was attributed to the appearance of extensive melt ponds that effectively transmit light to the water below (Arrigo et al. 2014). Yet, we still remain in the dark about the status of phytoplankton acclimation and production rates beneath snow-covered sea ice prior to melt-pond formation and ice retreat.

The primary goal of this study is to compare phytoplankton photophysiology prior to the spring bloom when light is limiting and nutrients are high (LLHN) and later in the summer when light levels are high but surface NO_3^- has been depleted (HLLN). To do so, we made a suite of photophysiological measurements that allowed us to characterize the specific strategies used by phytoplankton to acclimate to light limitation in the spring and nutrient limitation in the summer. This research was made possible by the creation of the first comprehensive dataset describing phytoplankton photophysiology beneath the expansive springtime sea ice in the Chukchi Sea.

METHODS

Chukchi Sea site

Hydrographic measurements in the Chukchi Sea were made during three field expeditions spanning 2010 to 2014, representing a variety of environmental conditions. The Impacts of Climate on EcoSystems and Chemistry of the Arctic Pacific Environment (ICESCAPE) project included two cruises from 18 June to 16 July 2010 and 28 June to 24 July 2011 onboard the United States Coast Guard Cutter *Healy*. ICESCAPE sampling surveyed the Chukchi Sea continental shelf during the late spring and early summer, which included stations in both ice-free and ice-covered water (Fig. 1). The Study of Under-ice Bloom In the Chukchi Ecosystem (SUBICE) campaign (13 May to 23 June 2014), also onboard the *Healy*, covered a similar geographic area to ICESCAPE (Fig. 1) but primarily surveyed under-ice hydrographic

conditions and phytoplankton communities, providing the most spatially extensive dataset of pre-bloom, ice-covered conditions in the northeastern Chukchi Sea collected to date. Together, these three expeditions to the Chukchi Sea provide a comprehensive dataset that chronicles pre- and post-bloom phytoplankton photophysiology and growing conditions, which include dramatic changes in ice cover, light and nutrient availability.

Hydrography

At each station, conductivity-temperature-depth (CTD) casts were conducted using temperature, conductivity, and pressure sensors (Sea-Bird electronics) attached to a 12-position 30-liter Niskin bottle rosette system. Discrete surface seawater samples were collected at standard depths of 2, 5, and 10 m. Chlorophyll *a* (Chl *a*), particulate organic carbon (POC), and fast repetition rate fluorometry (FRRf) were measured at each station and at each depth. High performance liquid chromatography (HPLC) pigments, photosynthesis vs irradiance (P-E) incubations, particulate absorption, and phytoplankton taxonomy were assessed at each station at the surface depth. Simulated in situ (SIS) measurements of primary production were measured at select stations over a 24 h period.

Nutrient analyses of unfiltered water samples were performed onboard the ship with a Seal Analytical continuous flow Auto-Analyzer 3 using a modification of the method described in Armstrong et al. (1967) to measure the concentrations of NO_3^-, ammonium (NH_4^+), nitrite (NO_2^-), phosphate (PO_4^{3-}), and silicate ($Si(OH)_4$) with detection limits of 0.02, 0.04, 0.02, 0.02, and 0.05 μM, respectively. Only NO_3^- data are presented here (Table 1).

Sea ice concentration

Daily satellite images from the Special Sensor Microwave Imager (SSM/I) at 25 km resolution were obtained from the National Snow and Ice Data Center (Cavalieri et al. 1996) and used to characterize the sea ice concentration at each station on the date of sampling. Sea ice concentration was also estimated visually through 'ice watch' observations every two hours made from the *Healy's* bridge using the ASSIST protocol (using the ASSIST protocol http://icewatch.gina.alaska.edu/). Because satellite ice concentrations correlated well with the dependent variable of in situ ice watch observations ($R=0.83$; slope=0.67; $p<0.01$), we used only satellite-derived sea ice concentrations in this study to represent a large spatial area surrounding each station (Lowry et al. 2018). Conservative thresholds of ice concentration were used to discern between completely ice-covered (>80%) and ice-free (<10%) environments.

Irradiance

Average incoming daily PAR (µEin m^{-2} s^{-1}; 400 to 700 nm) used to characterize seasonal variability was determined using the atmospheric radiative transfer model of Gregg and Carder (1990) and corrected for cloud cover (determined from NCEP Reanalysis data) (Figure 2).

During SUBICE, in situ downwelling PAR at solar noon was measured both above and below the ice cover using two RAMSES ACC-2 VIS TriOS hyperspectral radiometers at 3 nm resolution from 320 to 950 nm (Table 2). A surface reference sensor was mounted above the ice and a second sensor was attached to an extending arm that was sent down a borehole and floated to an upright position approximately 10 cm from the bottom of the ice and 2.5 meters (horizontally) from the borehole. Oriented towards the direction of the sun, five measurements made in 45° increments were collected in a clockwise fashion around the arc created by the 2.5 m radius of the sensor arm. Irradiance spectra were interpolated to 1 nm resolution. Any

inclinations greater than 10° from vertical were discarded. Spectral transmittance (T(λ)) was calculated as the percentage of downwelling irradiance at the surface that is measured underneath the ice as

$$T(\lambda) = \frac{F_t(\lambda)}{F_S(\lambda)} \times 100 \quad (1)$$

where $F_T(\lambda)$ is spectral downwelling irradiance underneath the ice and $F_S(\lambda)$ is spectral downwelling irradiance incident at the surface. PAR was calculated for each downwelling spectral irradiance observation below the ice cover by converting transmitted watts at each wavelength to number of photons between 400 and 700 nm. From a regression of all samples (n = 468), the conversion was empirically determined to be 4.475 µEin m^{-2} s^{-1} for total watts m^{-2} transmitted.

During the ICESCAPE cruises, in situ PAR was calculated from underwater vertical profiles measured by a free-falling Profiling Reflectance Radiometer (PRR; Biopherical Instruments Inc. PRR800/810) (Table 2). A PRR deployment consisted of three replicate casts conducted in ice-free waters at local noon. Mean in situ surface PAR representative of the LLHN and HLLN environments was calculated as the mean of all in situ radiometric measurements at solar noon for each environmental condition (Table 2).

Photophysiological measurements

Pigments and biomass

Chlorophyll a: Seawater samples were filtered onto 25 mm Whatman glass fiber filters (GF/F, 0.7 μm nominal pore size). Pigments of filters were extracted in the dark in 5 ml of 90% acetone for 24 h at +3°C prior to measurement on a Turner Designs 10-AU fluorometer calibrated with pure Chl *a* (Sigma-Aldrich) (Holm-Hansen et al. 1965). We opted to use fluorometric Chl *a* throughout this study because the majority of HPLC samples were lost during

the ICESCAPE 2010 cruise, restricting our ability to statistically compare any parameters that rely on Chl *a* concentration, including P-E, absorption, and growth rates.

Pigments: Samples for analysis of pigments were measured using HPLC. Pigment samples were immediately flash frozen in liquid nitrogen after filtration and stored at -80°C until analysis was performed within six months of collection at The Analytical Services Laboratory at Horn Point, Cambridge, MD, following Zapata et al. (2000) for ICESCAPE samples and at Laboratoire d'Océanographie de Villefranche (LOV) as described in Ras et al. (2008) for SUBICE samples.

Particulate organic carbon: Particulate organic carbon (POC) samples were filtered through 25 mm pre-combusted (450°C for 4.5 h) GF/Fs. Blank filters were measured daily by passing ~25 ml of filtered (0.2 μm) seawater through GF/Fs. Filters were immediately dried at 60°C and stored dry until processing. Prior to analysis, samples were fumed with concentrated HCl, dried at 60°C, and packed into tin capsules (Costech Analytical Technologies, Inc.) for analysis. Samples were analyzed on an Elementar Vario EL Cube or Micro Cube elemental analyzer (Elementar Analysensysteme GmbH, Hanau, Germany) interfaced to a PDZ Europa 20-20 isotope ratio mass spectrometer (Sercon Ltd., Cheshire, UK).

Taxonomy

Community composition of surface water samples was assessed onboard the ship using Imaging FlowCytobot (IFCB) analysis to determine the relative contributions (mean ± SD) of algal taxa, following the methods in Selz et al. (2017). Phytoplankton in small volumes of seawater (1 to 5 ml) were injected through a cytometry flow cell (860 x 180 µm) and each Chl *a*-containing particle (chain, colony, or cell) triggered the digital camera. The IFCB cell-size

detection range was limited to roughly 8 to 300 μm. All digital micrographs were classified to the genus level both manually and assisted by the supervised machine learning strategy discussed in Laney and Sosik (2014). Phytoplankton genera were then sorted into broader taxonomic categories based on categorization used in Laney and Sosik (2014): pennate diatoms (*Cylindrotheca, Entomoneis, Ephemera, Fragilariopsis, Gyrosigma, Haslea, Navicula, Nitzschia, Pinnularia, Pleurosigma, Pseudo-nitzschia, Rhizosolenia, Thalassionema*), centric diatoms (*Attheya, Bacterosira, Chaetoceros, Coscinodiscus, Detonula, Eucampia, Guinardia, Leptocylindrus, Melosira, Odontella, Paralia, Skeletonema, Thalassiosira, Lauderia*), flagellates (*Dictyocha, Dinobryon, Euglena, Phaeocystis, Pyramimonas*), dinoflagellates, ciliates, small unidentified cells, large unidentified cells, and detritus. Small and large cells that we were unable to identify due to irregular shape or poor image quality and were classified as "unidentified" and categorized using an approximate size cut off of less than or greater than 10 μm. The relative abundance of each taxonomic category was based on number of images recorded relative to the total images.

Variable fluorescence

Phytoplankton physiology was assessed using a fast repetition rate fluorometer (FRRf; LIFT-FRR, Soliense; Kolber et al. 1998a) with excitation at 470 nm to estimate the maximum photochemical efficiency of photosystem II (F_v:F_m; dimensionless), functional absorption cross-section (σ_{PSII}; $Å^2$ $quanta^{-1}$), and turnover time of the primary electron acceptor at PSII (τ_{PSII}; ms). The samples were dark-acclimated for ~30 minutes at 0°C and measured in triplicate within one hour of collection. Blanks for individual samples analyzed by FRRf were prepared by gentle

filtration through a 0.2 mm polycarbonate syringe filter before measurement using identical protocols. All reported values were corrected for blank effects.

Photosynthesis vs. irradiance

Photosynthesis vs. irradiance (P-E) relationships were measured using a short-term ^{14}C-bicarbonate ($H^{14}CO_3^-$) incorporation technique (Lewis and Smith 1983). Briefly, for each P-E curve, samples were spiked with $H^{14}CO_3^-$ and incubated in photosynthetron at 14 light intensities ranging from 1 to ~600 µEin m^{-2} s^{-1}. Even illumination was provided to each incubation chamber via a fiber-optic cable connected to an illuminator (Lumenyte International Corporation, model DMX512) fitted with a 150 W tungsten-halogen lamp. Total PAR within each illumination chamber was measured using a Biospherical Instruments Inc. QSL-2101. Spectral irradiance, $E(\lambda)$, was measured from 300 to 800 nm using a spectroradiometer (Analytical Spectral Devices, FieldSpec). Incubations were terminated after 2 h by turning off the light source and acidifying each vial. All acidified samples were gently shaken for a minimum of 12 h to drive off radioactive inorganic carbon. Radioactivity was determined by liquid-scintillation counting. For full detailed methods, please refer to Arrigo et al. (2010).

The carbon uptake rates were calculated using a nonlinear least-squares regression fit to the relationship of Platt et al. (1980), as modified by Arrigo et al. (2010)

$$P^* = P_S^* \left(1\text{-}e^{\frac{-\alpha^* E}{P_S^*}}\right) e^{\frac{-\beta^* E}{P_S^*}} \text{-} P_0^* \qquad (2)$$

where P^* is the measured Chl *a*-specific photosynthetic rate (mg C mg^{-1} Chl *a* h^{-1}) at a given photosynthetron irradiance *E* (µEin m^{-2} s^{-1}), P^*_s is the light saturated photosynthetic rate (mg C

mg^{-1} Chl *a* h^{-1}) in the absence of photoinhibition, α^* (mg C mg^{-1} Chl *a* h^{-1} (µEin m^{-2} s^{-1})$^{-1}$) is the initial slope of the P-E curve, β^* is the photoinhibition term (mg C mg^{-1} Chl *a* h^{-1} (µEin m^{-2} s^{-1})$^{-1}$), and P^*_0 is the CO_2 uptake or release (mg C mg^{-1} Chl *a* h^{-1}) at E = 0 µEin m^{-2} s^{-1}. P-E parameters were only used when the fits were statistically significant (r^2 >0.70 and p <0.05). The maximum photosynthetic rate (P^*_{max}; mg C mg^{-1} Chl *a* h^{-1}) was calculated as

$$P^*_{max} = P^*_s\left(\frac{\alpha^*}{\alpha^*+\beta^*}\right)\left(\frac{\beta^*}{\alpha^*+\beta^*}\right)^{\frac{\beta^*}{\alpha^*}} \quad (3)$$

and the photoacclimation parameter E_k (µEin m^{-2} s^{-1}) was calculated as

$$E_k = \frac{P^*_{max}}{\alpha^*}. \quad (4)$$

Absorption

Spectral light absorption by particulates (phytoplankton and detritus) was determined using two different methods for ICESCAPE and SUBICE cruises. A water sample was immediately filtered after sampling using a GF/F filter for both cruises. For ICESCAPE, the filter was then stored in a liquid nitrogen and brought back to the laboratory at Scripps Institute of Oceanography. Absorbance of a sample filter was measured at 1 nm resolution (300–800 nm) using a dual-beam spectrophotometer (Perkin-Elmer-Lambda-18) equipped with an integrating sphere. The filter was placed in the middle (inside) of the integrating sphere (Rötggers and Gehnke 2012) and an appropriate beta factor for correcting pathlength amplification due to the filter and particles, dedicated to the specific geometry, was used to calculate absorption coefficients of particles (Neukermans et al. 2014). For SUBICE, absorbance was measured onboard using a Varian Cary 100 spectrophotometer by placing a sample filter in front and back of an integrating sphere (so-called Transmittance-Reflectance or T-R method; Tassan and Ferrari 1995). An appropriate beta factor for this specific geometry was used to calculate absorption coefficients of particles (Tassan and Ferrari 2002).

Absorption by phytoplankton (a_{ph}) was calculated as the difference between the particulate (a_p) and detrital (a_d) absorption coefficients (m^{-1}). The Chl *a*–specific spectral absorption coefficient for phytoplankton (a^*_{ph}, m^2 mg^{-1} Chl *a*) is a_{ph} normalized to fluorometrically determined Chl *a*. The red and blue absorption peak of the Chl *a* spectrum was determined as the maximum value between 650-680 and 450-480 nm, respectively. The spectrally averaged Chl *a*–specific absorption coefficient for phytoplankton ($\bar{a}^*$, m^2 mg^{-1} Chl *a*) was then calculated as

$$\bar{a}^* = \frac{\sum_{700}^{400} a^*_{ph}(\lambda) \times E(\lambda)}{\sum_{700}^{400} E(\lambda)} \quad (5)$$

where $E(\lambda)$ is the spectral output of the P-E photosynthetron light source.

Quantum yield

The maximum quantum yield of photosynthesis, Φ_m, was calculated from α* and $\bar{a}^*$ as

$$\phi_m = \frac{\alpha^*}{43.2 \times \bar{a}^*} \quad (6)$$

where 43.2 represents a unit conversion to mol C (mol quanta absorbed)$^{-1}$ (SooHoo et al. 1987).

Phytoplankton growth rates

Maximum biomass-specific daily growth rate (μ_m; d^{-1}) for a given sample was calculated as

$$\mu_m = P^*_{max} \times \frac{Chl\,a}{POC} \times 24\,. \quad (7)$$

Mean biomass-specific daily growth rate (μ_{avg}; d^{-1}) was calculated using P-E parameters from (Eq. 3) at the mean in situ surface PAR representative of the LLHN or HLLN environment (Table 2).

$$\mu_{avg} = \frac{\alpha^* \times E}{POC{:}Chl\,a} \times 24\,. \quad (8)$$

Primary production

Simulated in situ (SIS) measurements of PP (mg C m^{-2} d^{-1}) were performed by measuring the uptake of labeled C-bicarbonate in water samples incubated over a 24 h period. Samples were incubated in a simulated water column light environment in continuous flow tanks on deck so that the phytoplankton were kept at in situ water temperature.

During the SUBICE cruise, water was collected at 4 depths (typically 2, 10, 25 and 45 m). Samples in 500 ml polycarbonate flasks were spiked with ^{13}C-bicarbonate and incubated beneath a cover that reduced incoming PAR to replicate a 1 m ice layer in flasks screened with layers of neutral density mesh that best matched their in situ light based on percentage of surface irradiance detected by the PAR sensor attached to the CTD rosette (25, 15, 8.8, 5.5, 3.3, 2.0, or 0.3% of surface light). We added 510 µL of a solution of 20 g L^{-1} of sodium bicarbonate ($NaH^{13}CO_3^-$) in the 500 ml incubation bottles. After a 24 h incubation, ^{13}C enrichment of the particulate matter collected onto 25 mm GF/Fs filters was analyzed by mass spectrometry at Université Laval (for full methods, see Tremblay et al. 2006).

During ICESCAPE, water was collected at 4 depths (typically 2, 10, 25 and 45 m) and incubated at corresponding light intensities. We added 0.74 MBq $H^{14}CO_3^-$ to 150 ml of sample in a 250 ml Falcon flask and covered the flask with 0 to 9 layers of neutral density screens to simulate light intensities of 85, 65, 25, 10, 5 and 1% of surface irradiance. After incubation, 30 ml of sample was filtered onto 25 mm GF/Fs in triplicate under very low vacuum (< 5 mm Hg). Filters were acidified with 0.1 ml of 6 N HCl to drive off inorganic C. After 24 h of acidification, 5 ml of scintillation cocktail (Ecolume) was added and samples were counted after >3 h on a

PerkinElmer Tri-Carb liquid scintillation counter. Total activity was determined for each sample by adding 50 µl of sample to 50 µl of ethanolamine, 0.5 ml of filtered seawater, and 5 ml of scintillation cocktail. Time zero controls were filtered (30 ml in triplicate), acidified at the start of the incubation period and then subtracted from the counts.

To calculate depth-integrated PP, total activity was converted to carbon uptake (mg m^{-3} d^{-1}) and was then integrated over the water column to achieve rates of daily PP (mg m^{-2} d^{-1}).

Environmental classifications

In order to compare the two environmental extremes experienced by Chukchi Sea phytoplankton, surface samples were classified as either low-light, high-nutrient (LLHN) or high-light, low-nutrient (HLLN) based on thresholds of ice concentrations and NO_3^- (Table 3).

Concentrations of NO_3^-, the limiting nutrient for phytoplankton growth in the AO, are dramatically reduced as the growing season progresses. Beneath the sea ice in spring, prior to the annual phytoplankton bloom, NO_3^- is >8 μM throughout the water column at all stations sampled across the Chukchi Sea shelf (Arrigo et al. 2017). After the phytoplankton bloom, NO_3^- is reduced to undetectable levels in surface water (Lowry et al. 2015). To characterize the seasonal extremes of NO_3^- available to phytoplankton, a conservative cutoff of >3 μM and < 1 μM was used to determine high-nutrient and low-nutrient conditions, respectively.

When determining light availability for phytoplankton, there is a distinct seasonal difference associated with changing ice cover. Perhaps surprisingly, average incoming daily PAR exhibited only a modest seasonal cycle during our study period (Fig. 2). Average incoming PAR during spring (391 ± 74 µEin m^{-2} s^{-1}) was not statistically different from summer (406 ± 60 µEin m^{-2} s^{-1}), with the amount of day-to-day variation in incoming PAR comparable to the

variation between average spring and summer incoming PAR (Fig. 2). However, during the spring SUBICE cruise, the majority of stations were covered by sea ice and snow with average thicknesses of 1.23 ± 0.22 m and 0.07 ± 0.05 m, respectively, with no melt ponds present (Selz et al. 2017). During the summer ICESCAPE cruises, most stations (and all of those considered in this study) were in open water. The seasonal differences in underwater light availability reflect the seasonal difference in ice cover: PAR beneath the sea ice in spring measured at solar noon was 14.50 ± 18.13 μEin m^{-2} s^{-1}, which was only 2% of the mean measured surface PAR at solar noon (762.73 ± 143.55 μEin m^{-2} s^{-1}) in the summer open water conditions (Table 2). The 2% transmission factor is comparable with other measurements (Laney et al. 2017) and modeled estimates (Pavlov et al. 2017) for ice cover in this region. Thus, this seasonal difference in surface PAR is attributable to attenuation by sea ice, snow and ice algae during spring (Selz et al. 2017; Arntsen 2018). The dramatic increase in surface PAR upon the disappearance of sea ice combined with the small seasonal variation in incoming solar radiation supports prior research that the presence of sea ice and snow is the main control on light availability for phytoplankton (Tremblay and Gagnon 2009; Perovich and Polashenski 2012; Lowry et al. 2018). Therefore, ice concentration was used to categorize low-light (>80% ice cover) or high-light (<10% ice cover) underwater environments.

LLHN samples include measurements from the spring SUBICE expedition at stations where ice cover was >80% and surface NO_3^- was >3 μM. HLLN samples are from the two ICESCAPE expeditions during summer at stations where ice cover was <10%, surface nitrate was <1 μM and sample depth was shallower than the mixed layer depth (MLD) to ensure upper mixed layer samples only. We also sorted samples to consider high-light high-nutrients (HLHN) and low-light low-nutrient (LLLN); however, there were too few samples for robust statistical

analysis, so we proceeded by analyzing only the two seasonal extremes (LLHN, HLLN) (Table 3). Because the sampling areas of SUBICE and ICESCAPE did not perfectly overlap, we repeated our analyses using only those stations that were approximately collocated during both SUBICE and ICESCAPE and the results did not differ from when we used all the stations from both field programs. However, because we did not want to reduce our sample size by eliminating stations, we elected to base our conclusions on the full datasets.

Statistical analysis

Low-light, high-nutrient springtime (LLHN) and high-light, low-nutrient summer (HLLN) data were compared using a Welch's two sample *t*-test. Differences were considered significant when the p-value was < 0.05. Results of the statistical analyses, including mean ± standard deviation, n, t-statistic and p-value, are reported in Table 4.

RESULTS

Phytoplankton community

Diatoms dominated the phytoplankton community, accounting for at least 60% of the total population during both seasonal conditions, although the taxonomic composition of the diatoms differed. In the pre-bloom, light limited spring (LLHN), the phytoplankton community was dominated numerically by pennate diatoms (39%), with centric diatoms accounting for 21%. The remaining fraction of the community was comprised of flagellates (16%), dinoflagellates (6%), and unidentified small (10%) and large cells (8%). During the post-bloom HLLN period, the taxonomic composition of the diatoms switched: centric diatoms dominated both the total phytoplankton community (62%) and the diatom community (90%), with pennate diatoms

making up a much smaller portion (7% of total phytoplankton, 10% of diatoms). Dinoflagellates (16%) and ciliates (11%) increased in proportion, while flagellates (4%) decreased in relative abundance. It is important to note, however, that the IFCB cannot reliably detect cells smaller than 8 μm, so the observed changes may not reflect changes in the smallest size class of phytoplankton (Laney and Sosik 2014). However, changes in pigments can reveal changes in taxonomy (Coupel et al. 2015). For example, in the Western Arctic, changes in Chl *b*/Chl *a* and 19'- hexanoyloxyfucoxanthin/Chl *a* indicate changes in small green algae and nanoflagellates, respectively (Coupel et al. 2015). Between the LLHN and HLLN, there was no significant difference in either pigment ratios, indicating that there was not a significant increase or decrease in the contribution of total chlorophyll by small cells undetectable by the IFCB. The seasonal transition of phytoplankton communities in the Chukchi Sea is discussed further in Selz et al. (2017).

Pigments and absorption of light

Absorption of light. The spectrally-integrated mean Chl *a*-specific absorption coefficient ($\bar{a}^*$, m^2 mg^{-1} Chl *a*), a measure of how much total light energy is absorbed per unit Chl *a*, significantly increased as phytoplankton transitioned from a LLHN environment (0.014 ± 0.019 m^2 mg^{-1} Chl *a*) to a HLLN environment (0.029 ± 0.023 m^2 mg^{-1} Chl *a*) as a result of a reduction in the degree of pigment packaging (Table 4). As phytoplankton are exposed to higher light, less Chl *a* is packed into each cell, thereby decreasing the overall light absorbed by the cell, but increasing absorption on a per Chl *a* basis (i.e., higher $\bar{a}^*$).

Pigment packaging. Because the effects of pigment packaging are stronger at wavelengths where Chl *a* absorbs most effectively (blue and red), the degree of pigment

packaging is characterized by a relative flattening of the blue and red absorption peaks, with ratios of blue to red absorption (a^*_{ph} blue:red) closer to 1 indicating stronger pigment packaging (Morel and Bricaud 1981). In the ice-covered LLHN and open water HLLN environments, a^*_{ph} blue:red averaged 2.02 ± 0.65 and 2.69 ± 0.69, respectively (Table 4), indicating a greater degree of packaging beneath the sea ice. The cellular POC to Chl *a* ratio (POC:Chl *a*) provides another indication of pigment packaging (Falkowski and Raven 2007). While Chl *a* concentration did not change between seasonal conditions (LLHN 1.71 ± 1.96, HLLN 1.53 ± 4.44 mg Chl *a* m^{-3}) (Table 4), POC significantly increased, resulting in a significant increase in POC:Chl *a* from LLHN (119 ± 120 g:g) to HLLN (314 ± 170 g:g) conditions, which further supports the observation of reduced pigment packaging by phytoplankton upon exposure to ice-free waters (Table 4). However, some of the POC can be comprised of non-phytoplankton material, like detritus or heterotrophic organisms, which could affect our analysis. Fortunately, nonalgal matter contributed only ~20% of the total POC in both seasons and did not exhibit a noticeable seasonal signal. Similarly, in another study in the Western Arctic, observed a^*_{ph} declined significantly from the ice melt period in the early spring to the summer and was attributed to the strong pigment packaging effect that overwhelmed the influence of the pigment composition (Matsuoka et al. 2011).

Photoprotective and photosynthetic pigments. Photosynthetic accessory pigments (PSP) aid Chl *a* in increasing light absorption. As phytoplankton transitioned from the light-limiting environment beneath the ice (LLHN) to the high light of summer (HLLN), phytoplankton significantly decreased cellular concentrations of PSP (19'-butanoyloxyfucoxanthin, 19'-hexanoyloxyfucoxanthin, fucoxanthin, peridinin, prasinoxanthin). PSP normalized by Chl *a*

significantly decreased from 0.482 ± 0.046 g:g in LLHN to 0.320 ± 0.089 g:g in HLLN (Table 4).

Coinciding with the relative decrease in PSP, phytoplankton significantly increased cellular concentrations of photoprotective xanthophyll pigments (PPP). Non-photochemical quenching (NPQ), the thermal dissipation of excess energy by PPP, protects phytoplankton cells against damage from excess incoming energy (Olaizola et al. 1994). Upon exposure to damaging levels of light, epoxidated xanthophyll pigments (e.g., diadinoxanthin (DD) and violaxanthin (vio)) are rapidly converted via a reversible, light-driven reaction to their de-epoxidated form (diatoxanthin (DT) and zeaxanthin (zea), respectively). The de-epoxidated form of the pigment preferentially absorbs and dissipates excess excitation energy, thereby preventing overexcitation and photoinhibition within the PSII reaction center (Olaizola et al. 1994). Concentrations of photoprotective xanthophyll pigments (PPP = DD + DT + vio + zea) normalized by Chl *a* doubled as phytoplankton transitioned from the LLHN environment (0.074 ± 0.017 g:g) to the HLLN environment (0.153 ± 0.065 g:g; Table 4). Paralleling the significant increase in PPP, phytoplankton also significantly increased concentrations of nonphotosynthetic carotenoids (NPC = zea + DD + alloxanthin + β-carotene) normalized by Chl *a* from 0.11 ± 0.025 g:g in LLHN spring to 0.32 ± 0.069 g:g in HLLN summer, consistent with the trends observed during the study of Matsuoka et al. (2011).

Active fluorescence

Between seasons, there was no significant change in F_v:F_m (LLHN 0.43 ± 0.13, HLLN 0.39 ± 0.11; Table 4), a measure of photochemically competent PSII centers (Behrenfeld et al. 1998; Sugget et al. 2010). The functional absorption cross-section of PSII (σ_{PSII}, $Å^2$ $quanta^{-1}$)

reflects the capacity of PSII antenna pigments to harvest and transfer light energy in order to undergo a photochemical reaction, while maximum turnover time (τ_{PSII}, ms) is the amount of time required to transport an electron through PSII (Sugget et al. 2010). In LLHN conditions, relatively slow τ_{PSII} (1.01 ± 0.23 ms) co-occurred with a relatively large σ_{PSII} (497 ± 83.5 $Å^2$ $quanta^{-1}$, Table 4). In contrast, for phytoplankton in HLLN conditions, τ_{PSII} was significantly faster (0.79 ± 0.34 ms) than LLHN, coinciding with a significant decrease in σ_{PSII} (379 ± 101 $Å^2$ $quanta^{-1}$, Table 4).

Carbon fixation

P^*_{max}. The maximum Chl *a*-specific photosynthetic rate, determined from P-E relationships, expresses the maximum carbon fixation rates achievable by phytoplankton under ambient conditions. During the nutrient replete pre-bloom season (LLHN), phytoplankton achieved remarkably high P^*_{max} values of 2.42 ± 0.92 mg C mg^{-1} Chl *a* h^{-1} (Fig. 3, Table 4). However, despite higher available PAR (Table 2), P^*_{max} decreased by 70% between LLHN and HLLN conditions, to only 0.83 ± 0.45 mg C mg^{-1} Chl *a* h^{-1} (Fig. 3, Table 4).

α^*. The initial slope of the P-E curve, a measure of the photosynthetic efficiency (Raven 2007; Arrigo et al. 2010), was relatively high in the LLHN environment (0.043 ± 0.031 mg C mg^{-1} Chl *a* h^{-1} (µEin m^{-2} s^{-1})$^{-1}$, Fig. 3, Table 4). However, α^* was reduced significantly to 0.017 ± 0.016 mg C mg^{-1} Chl *a* h^{-1} (µEin m^{-2} s^{-1})$^{-1}$ (Fig. 3, Table 4) in the HLLN environment.

E_k. The photoacclimation parameter usually represents the light level to which phytoplankton are optimally acclimated (Falkowksi and Raven 2007). Although light levels experienced by the phytoplankton increased dramatically once sea ice retreated (Table 2), E_k was

nearly identical between the ice-covered spring (LLHN 67.8 ± 63.2 µEin m^{-2} s^{-1}) and the open-water summer (HLLN 68.5 ± 42.6 µEin m^{-2} s^{-1}).

β^*. The photoinhibition parameter quantifies the effects of photodamage upon exposure to supersaturating irradiance. Spring phytoplankton growing in the LLHN conditions suffered severe photoinhibition at irradiances above ~250 µEin m^2 s^{-1} (0.014 ± 0.024 mg C mg^{-1} Chl *a* h^{-1} (µEin m^{-2} s^{-1})$^{-1}$, Fig. 3, Table 4). Surprisingly, phytoplankton from the HLLN environment experienced significantly less photoinhibition at the same irradiances (0.0006 ± 0.0005 mg C mg^{-1} Chl *a* h^{-1} (µEin m^{-2} s^{-1})$^{-1}$, Fig. 3, Table 4).

Φ_m. The maximum quantum yield of photosynthesis represents the number of moles of CO_2 reduced for each mole of quanta absorbed. Any changes in the amount of absorbed energy that is used for carbon fixation will impact Φ_m. As the season progressed from LLHN to HLLN conditions, Φ_m was significantly reduced from 0.163 ± 0.089 to 0.020 ± 0.025 (Table 4).

Growth and carbon fixation rates. Both μ_{max} and μ_{avg} decreased significantly from the pre-bloom LLHN season to the post-bloom HLLN season (Table 4). μ_{max} decreased the most dramatically, from 1.31 ± 0.50 d^{-1} in LLHN spring to 0.09 ± 0.12 d^{-1} in the HLLN summer. These estimates of µ are conservative because some of the POC was comprised of non-phytoplankton particulate matter such as detritus, bacteria, heterotrophic protists, or metazoans, thereby leading to underestimates of phytoplankton growth rates. Approximately half of the observed decrease in μ_{max} from LLHN to HLLN conditions was driven by decreases in P^*_{max} and half by increases in POC:Chl *a* (Table 4). Similarly, μ_{avg} significantly declined from 0.27 ± 0.12 d^{-1} in LLHN to 0.07 ± 0.09 d^{-1} as phytoplankton transitioned to HLLN conditions during the summer (Table 4). Despite the significant decrease in growth rates between seasons, SIS daily PP rates exhibited no significant differences between LLHN and HLLN conditions (Table 4),

averaging 1.05 ± 0.99 and 2.5 ± 4.6 g C m^2 d^{-1}, respectively.

DISCUSSION

Phytoplankton photoacclimate to their environment by changing their cellular makeup and photosynthetic machinery, which can be characterized by measuring changes in a variety of photosynthetic and physiological parameters. In this study, we compared the changes in bulk physiology measured for the pre- and post-bloom phytoplankton communities in order to evaluate strategies used by phytoplankton to acclimate to either light or nutrient limitation. We deliberately ignored the peak bloom period when there is ample light and nutrients to support high, although short-lived, rates of production.

In both the spring and summer, diatoms dominated the phytoplankton community, consistent with previous studies in the region (Hsiao et al. 1977; Booth et al. 2002; Lovejoy et al. 2002; Hill et al. 2005; Brugel et al. 2009; Ardyna et al. 2011; Galindo et al. 2014). While some studies suggest that bulk phytoplankton photophysiological parameters are influenced by changes in community composition (Moore et al. 2006; Sugget et al. 2009), the consistency of diatom dominance between LLHN and HLLN conditions allowed us to focus on the impact of environmental changes on variations in photosynthetic parameters. However, for parameters that are known to have a particularly strong species-specific or cell-size effect (Moore et al. 2006; Sugget et al. 2009), such as functional absorption cross-section or pigment packaging, additional caution may be needed when attributing photophysiological changes to environmental controls.

Phytoplankton responses to light

Beneath the sea ice in spring when nutrients are plentiful (LLHN), phytoplankton displayed clear signs of low light photoacclimation. Phytoplankton increased intracellular concentrations of photosynthetic pigments (PSPs), which was supported by the abundant nutrients required for biosynthesis (Geider et al. 1993, 1998). In doing so, phytoplankton packed their cells with Chl *a* and other PSPs to maximize absorption of the limited light available beneath the sea ice, resulting in a low $\bar{a}^*$ (Morel and Bricaud 1981; Falkowski et al. 1985). As sea ice retreated, phytoplankton were exposed to much higher incoming light (Table 2). No longer requiring such effective light absorption, phytoplankton reduced their internal concentrations of Chl *a* and PSPs (MacIntyre et al. 2002; Kropuenske et al. 2009; Nymark et al. 2009; Arrigo et al. 2010), causing $\bar{a}^*$ to rise.

Simultaneously, phytoplankton increased their concentration of photoprotective pigments (PPPs) during HLLN to protect their photosynthetic machinery from damage by excess absorbed irradiance via non-photochemical quenching (NPQ). The up-regulation of PPPs in response to high light has previously been reported in polar phytoplankton, including diatoms, haptophytes and mixed populations (Hill et al. 2005; Van Leeuwe et al. 2005; Kropuenske et al. 2009; Nymark et al. 2009; Arrigo et al. 2010; Alderkamp et al. 2013). Any physiological changes that divert light energy away from carbon fixation, including dissipating absorbed light as heat or fluorescence (Babin et al. 1996), reduces Φ_m in proportion to increasing irradiance, regardless of nutrient concentration (Kiefer and Mitchell 1983; Falkowski et al. 1985). Mirroring the significant reduction in Φ_m, the Chl *a*-normalized photosynthetic efficiency (α^*) also significantly decreased in HLLN (Table 4). Although proportional to both $\bar{a}^*$ and Φ_m, α^* was largely controlled, in this case, by the large drop in Φ_m (Arrigo et al. 2010). Thus, the exchange

of photosynthetic pigments with photoprotective pigments dictated the concurrent increase in ā* and reduction of Φ_m and thus α^*.

The amount and type of pigments associated with the PSII reaction centers also govern the changes we observed in σ_{PSII} (Kolber et al. 1998b; Sugget et al. 2010). As phytoplankton transitioned from low light beneath sea ice to high light in open water, σ_{PSII} was significantly reduced to minimize light absorption (Falkowski et al. 1981). The drop in σ_{PSII} can be explained by the increase in NPQ and decrease in PSPs, the combined effect of which results in a photoacclimation strategy to lessen light absorption by the cell (Behrenfeld et al. 1998; Arrigo 2010; Trimborn et al. 2013). However, it is important to note that the range of variability in σ_{PSII} observable within diatom species can exceed the difference in σ_{PSII} measured between seasonal conditions (Moore et al. 2006; Sugget et al. 2009), so the impact of taxonomic changes between seasons also may impact the observed changes in σ_{PSII}.

Changes in pigment composition and σ_{PSII} were further reflected in τ_{PSII}. As phytoplankton expanded σ_{PSII} using enhanced PSPs to absorb more photons in spring, excitation energy would be expected to spend a longer time within the larger antennae before exiting PSII, thus slowing τ_{PSII}. However, as light levels increased, phytoplankton increased NPQ and thereby contracted σ_{PSII} in order to avoid photoinhibition, ultimately resulting in faster electron turnover in PSII (decreased τ_{PSII}). This trend agrees with previous observations that increasing irradiance drives decreases in τ_{PSII} due to a shrinking σ_{PSII} (Behrenfeld et al. 1998; Sugget et al. 2010). N-limitation, however, can increase τ_{PSII} due to constraints on the number of functional reaction centers (Kolber et al. 1988; Falkowski & Raven 2007). Thus, the overall decrease in τ_{PSII} in post-bloom conditions, despite N-limitation, suggests that the impact of increased light had a larger influence on τ_{PSII} and σ_{PSII} than did the effect of nutrient limitation.

A final low light acclimation response in the spring is seen in β^* (Fig. 3). Photoinhibition results when excess light energy damages proteins, lipids and pigments of the photosynthetic membrane (Moore et al. 2006; Kropuenske et al. 2009). Phytoplankton that were acclimated to LLHN conditions experienced significantly more photoinhibition at high irradiance than did phytoplankton acclimated to HLLN (Fig. 3, Table 4). It appears that by maximizing light absorption in the ice-covered environment, LLHN phytoplankton became especially susceptible to photoinhibition upon exposure to high irradiance (higher β^*, Fig. 3, Table 4). However, as surface PAR increased to potentially damaging levels (Table 2), the acclimation strategy of phytoplankton shifted to reduce light absorption and increase photoprotection, as evidenced by decreased PSPs and increased PPPs, thereby minimizing the risk of photoinhibition at high irradiances (lower β^*).

Nutrient limitation in summer

Attaining high rates of carbon fixation relies on sufficient incoming light energy and adequate synthesis of photosynthetic machinery that requires nutrients (Falkowski and Raven 2007). Early in the LLHN season, high nutrients permitted elevated P^*_{max}, despite low light beneath the sea ice (Tables 1, 2 and 4). As the ice receded and incoming PAR increased, P^*_{max} would be expected to increase even further as long as nutrients were available in surface waters (Nymark et al. 2009). However, after the seasonal peak in phytoplankton biomass, NO_3^- limitation ultimately controlled photosynthetic capacity (Moore et al. 2003; Hill et al. 2005; Tremblay et al. 2006; Palmer et al. 2013). Despite higher available irradiance, severe NO_3^- depletion after the peak bloom constrained P^*_{max} to relatively low rates during the HLLN season (Tables 1 and 4), comparable to other measurements made under nutrient limiting conditions (<1

mg C mg^{-1} Chl *a* h^{-1}) (Hill and Cota 2005). Nitrogen limitation constrains synthesis of nitrogen-containing biomolecules, including the proteins of the PSII and PSI reaction centers as well as carbon-fixation enzymes such as RUBISCO (Geider et al. 1993). In doing so, nitrogen limitation reduces the number of functional reaction centers (Kolber et al. 1998b), which consequently decreases photochemical energy conversion, as evidenced by lower P^*_{max} (Berges et al. 1996; Berges and Falkowski 1998; Litchman et al. 2002; van der Poll et al. 2005). Despite low levels of nitrogen, diatoms outcompete other taxa by efficiently extracting whatever NO_3^- remains through adaptions such as high nutrient affinity (Tambi et al. 2009), large NO_3^- storage vacuoles (Stolte and Riegmann 1995), and favorable morphologies that allow for efficient nutrient diffusion (Karp-Boss and Boss 2016).

In restricting P^*, NO_3^--limitation likewise limits phytoplankton growth rate (Table 4). Maximum growth rates calculated using P^*_{max} (μ_{max}) mirrored the significant decline in photosynthetic rates (Table 4). However, when considering rates based on average surface light at solar noon during each seasonal condition (Table 2), the mean photosynthetic rate (P^*) was similar (~0.6 mg C mg^{-1} Chl *a* h^{-1}) for both LLHN and HLLN environments (Fig. 3). Yet, because the POC:Chl *a* ratio had significantly increased later in the season due to reduced pigment packaging (Table 4), μ_{avg} significantly declined. While the increase in POC:Chl *a* could in part reflect either an increase in detrital matter or a change in cell size, the coincident increase in $\bar{a}^*$ and the a^*_{ph} blue:red ratio indicates that the change in POC:Chl *a* likely reflects the change in pigment packaging. So, despite the consistency of the photosynthetic rate between LLHN and HLLN seasons, μ_{avg} was significantly lower under HLLN conditions because of the increased POC:Chl *a* content of the cell.

Our results also suggest that nutrient limitation inhibits the ability of phytoplankton to acclimate to increased light availability in the summer. The surface PAR experienced by post-bloom phytoplankton at solar noon (762.73 ± 143.55 µEin m^{-2} s^{-1}; Table 2) was ~11 times greater than the light level to which they were supposedly acclimated (HLLN E_k 68.5 ± 42.6 µEin m^{-2} s^{-1}; Table 4). Assuming a diffuse attenuation coefficient (K_d) of 0.1 m^{-1} and an average MLD of 10 m representative of the HLLN summer, average PAR within the MLD at solar noon (~250 µEin m^{-2} s^{-1}) is still more than double the summer phytoplankton E_k (Table 4). In a recent study of Arctic phytoplankton photophysiology, Alou-Font et al. (2016) also observed that surface mixed layer irradiances above 600 µEin m^{-2} s^{-1} were associated with low cell viability and a decline in photosynthetic performance. The observed coincident drop in our study in both α^* and P^*_{max} between the light limited spring and nutrient limited summer results in a constant E_k, a phenomenon described as "E_k-independent" variability (Behrenfeld et al. 2004) (Fig. 3). Early in the season (LLHN), replete nutrients allowed for the synthesis of photosynthetic machinery required to photosynthesize efficiently at low light, which resulted in relatively high α^* and P^*_{max} (Behrenfeld et al. 2004). However, as the environment shifted to HLLN conditions and phytoplankton no longer required such efficient absorption (lower α^*), the manufacturing of photosynthetic machinery and subsequent production of reductants was impeded due to nutrient limitation (lower P^*_{max}) (Behrenfeld et al. 2004). So while in general, well-acclimated phytoplankton exhibit values for E_k that match the mean light field under which they were growing, our data suggest this is only true when nutrients are in ample supply.

Pre-bloom phytoplankton are primed to bloom

Supported by the high availability of nutrients, phytoplankton beneath snow-covered sea ice effectively acclimated to the low light environment to achieve high photochemical efficiencies and PP rates (Table 4). Pre-bloom F_v:F_m (0.43 ± 0.13) was comparable to that of polar phytoplankton during peak bloom periods (F_v:F_m 0.5-0.6; Gervais et al. 2002; Suzuki et al. 2002; McMinn and Hegseth 2004; Arrigo et al. 2014; Alou-Font et al. 2016), demonstrating that pre-bloom phytoplankton maintained high efficiency of electron flow through PSII. Even more surprising, rates of pre-bloom PP (1.05 ± 0.99 g C m^2 d^{-1}) were close to rates measured during the peak-bloom period (1.2-4.8 g C m^{-2} d^{-1}, Arrigo et al. 2014), suggesting that phytoplankton were able to achieve relatively high levels of PP regardless of the very low light levels.

Prior to the recent observation of a massive under-ice bloom (Arrigo et al. 2014), high rates of phytoplankton production have generally been assumed to be limited to open waters subsequent to sea ice retreat (Sakshaug 2004; Hill and Cota 2005; Perrette et al. 2011). Our study shows that despite >1 m thick, snow-covered sea ice (Selz et al. 2017), phytoplankton effectively acclimated such that low irradiance did not prevent phytoplankton growth. Consequently, current NPP estimates based solely on satellite-derived open water rates likely drastically underestimate annual AO NPP (Arrigo et al. 2014; Lowry et al. 2014). This under-ice, NO_3^--based "new" production is ecologically important because it is the fraction of NPP that is exported from the euphotic zone and can thus support the rich benthic community of the Chukchi Shelf (Fortier et al. 2002; Gruber 2008).

Not only are under-ice phytoplankton effectively acclimated to very low available light, their photophysiological parameters suggest that phytoplankton are "primed" to grow rapidly once light levels increase. Pre-bloom phytoplankton were capable of achieving exceptionally high rates of photosynthesis (Fig. 3). In fact, the mean P^*_{max} achieved by pre-bloom

phytoplankton beneath the sea ice (2.4 mg C mg^{-1} Chl *a* h^{-1}) is significantly higher than P^*_{max} measured during the under-ice phytoplankton bloom (Arrigo et al. 2014) and under other high-nutrient AO conditions (Hameedi 1978; Palmer et al. 2011, 2013). Because P^*_{max} is only achieved at light levels far greater (~200 µEin m^{-2} s^{-1}) than those beneath the ice (~14 µEin m^{-2} s^{-1}), under-ice phytoplankton appear to be primed to respond to the onset of increased light. The steep α^*, typical of low light environments, paired with the unexpectedly high P^*_{max}, allows phytoplankton to achieve great gains in photosynthetic rates for any small increase in light (Fig. 3). Similar to previous observations in AO ice algae and phytoplankton in open water leads (McMinn and Hegseth 2004; Gradinger 2009), the resultant E_k is higher than the average light experienced by the phytoplankton, supporting the idea that phytoplankton are prepared for future increases in light (Table 4).

This acclimation strategy provides phytoplankton with an advantage in the under-ice environment. While the mean light environment beneath the ice is very low (Table 2), it is also extremely variable due to patchy snow cover (Perovich et al. 1998), open water leads throughout the sea ice (Assmy et al. 2017; Lowry et al. 2018), and convective mixing of the water column (Pickart et al. 2016). The unexpectedly high P^*_{max} paired with high α^* enables phytoplankton to maximize production in response to rapid changes in the variable light environment. This acclimation response also provides phytoplankton a competitive advantage to utilize the fleeting nutrient reservoir immediately once light levels increase seasonally through melt pond formation (Frey et al. 2011), ice melt (Tremblay and Gagnon 2009) and/or the shoaling of the mixed layer (Strass and Nöthig 1996). Thus, this acclimation strategy is likely what allowed diatoms, in particular centric diatoms, to outcompete other taxa and dominate an increasingly large fraction of the phytoplankton community as the season progressed.

This strategy is consistent with previous studies demonstrating that diatoms thrive and dominate in highly variable light environments (Lavaud 2007). In dynamic light conditions, diatoms tend to maximize carbon fixation rates, despite the increased susceptibility to photoinhibition (Behrenfeld et al. 1998; Van Leeuwe et al. 2005). In doing so, high growth rates allow diatoms to outcompete other taxa, even if they are photodamaged in the process (Van Leeuwe et al. 2005).

This strategy of elevated growth rates in low light environments may favor diatom dominance in the future. Climate change is expected to continue impacting seasonal sea ice characteristics on Arctic shelves (IPCC 2014); multi-year sea ice will increasingly be replaced by thin first-year sea ice that melts earlier in the spring and is more prone to melt pond formation with dramatic consequences for the under-ice light environment (Maslanik et al. 2007; Stroeve et al. 2014). Thus, phytoplankton that are primed with high P^*_{max} and α^* will be better acclimated to future changes in the light beneath the sea ice.

REFERENCES

Alderkamp, A., M.M. Mills, G. van Dijken, and K.R. Arrigo. 2013. Photoacclimation and non-photochemical quenching under in situ irradiance in natural phytoplankton assemblages from the Amundsen Sea, Antarctica. Mar. Ecol. Prog. Ser. 475: 15-34, doi: 10.3354/meps10097

Alou-Font , E., S. Roy, S. Agustí, and M. Gosselin. 2016. Cell viability, pigments and photosynthetic performance of Arctic phytoplankton in contrasting ice-covered and open-water conditions during the spring−summer transition. Mar. Ecol. Prog. Ser. 543:89-106.

Ardyna, M., M. Gosselin, C. Michel, M. Poulin, and J-É. Tremblay. 2011. Environmental forcing of phytoplankton community structure and function in the Canadian High Arctic: contrasting oligotrophic and eutrophic regions. Mar. Ecol. Prog. Ser. 442: 37-57, doi: 10.3354/meps09378

Arntsen, A.E. 2018. Impacts of Changing Sea Ice in the Beaufort and Chukchi Seas. (Doctoral Thesis). Dartmouth College, Hanover, New Hampshire. Retrieved from https://search.proquest.com/openview/a1838f4d0b7dcf678603b07ed3c89969/1?pq-origsite=gscholar&cbl=18750&diss=y

Armstrong, F., C.R. Stearns, and J. Strickland. 1967. The measurement of upwelling and subsequent biological process by means of the Technicon Autoanalyzers and associated equipment. Deep-Sea Res. 14, 381–389. doi: dx.doi.org/10.1016/ 0011 7471(67)90082-4

Arrigo, K.R., G.L. van Dijken, and S. Bushinsky. 2008. Primary production in the Southern Ocean, 1997-2006. J. Geophys. Res. 113: C008004. doi: 10.1029/2007JC004551

Arrigo, K.R., M.M. Mills, L.R. Kropuenske, G.L. van Dijken, A.C. Alderkamp, and D. H. Robinson. 2010. Photophysiology in two major Southern Ocean phytoplankton taxa: Productivity and growth of *Phaeocystis antarctica* and *Fragilariopsis cylindrus* under constant irradiance. Integr. Comp. Biol. 50: 950–966, doi:10.1093/icb/icq021

Arrigo, K. and others. 2014. Phytoplankton blooms beneath the sea ice in the Chukchi Sea. Deep-Sea Res. Part II. 105: 1-16, doi: dx.doi.org/10.1016/j.dsr2.2014.03.018

Arrigo, K.R., M.M. Mills, G.L. van Dijken, K.E. Lowry, R.S. Pickart, and R. Schlitzer. 2017. Late spring nitrate distributions beneath the ice-covered northeastern Chukchi Shelf. J. Geophys. Res. 122: 2408-2417, doi: 10.1002/2017JG003881

Assmy, P. and others. 2017. Leads in Arctic pack ice enable early phytoplankton blooms below snow-covered sea ice. Sci. Rep. 7: 40850, doi: 10.1038/srep40850

Babin, M.A. Morel, H. Claustre. A. Bricaud. Z. Kolber, and P.G. Falkowski. 1996. Nitrogen- and irradiance-dependent variations of the maximum quantum yield of carbon fixation in eutrophic, mesotrophic and oligotrophic marine systems. 43: 1241-1272.

Behrenfeld, M.J., O. Prasil, Z.S. Kolber, M. Babin, and P.G. Falkowski. 1998. Compensatory changes in Photosystem II electron turnover rates protect photosynthesis from photoinhibition. Photosynth. Res. 58: 259-268.

Behrendfeld, M.J., O. Prasil, M. Babin, and F. Bruyant. 2004. In search of a physiological basis for covariations in light-limited and light-saturated photosynthesis. J. Phycol. 40:4-25.

Berges, J.A., D.O. Charlebois, D.C. Mauzerall, and P.G. Falkowski. 1996. Differential Effects of Nitrogen Limitation on Photosynthetic Efficiency of Photosystems I and II in Microalgae. Plant Physiol. 110:599-696. doi: https://doi.org/10.1104/pp.110.2.689

Berges, J.A. and P.G. Falkowski. 1998. Physiological stress and cell death in marine phytoplankton: Induction of proteases in response to nitrogen or light limitation. Limnol. Oceanog. 43: 129-135.

Booth, B.C., P. Larouche, S. Bélanger, B. Klein, D. Amiel, and Z.P. Mei. 2002. Dynamics of Chaetoceros socialis blooms in the North Water. Deep-Sea Res. Part II. 49: 5003–5025.

Brown, Z. W., K.L. Casciotti, R.S. Pickart, J.H Swift, and K.R. Arrigo. 2015. Aspects of the marine nitrogen cycle of the Chukchi Sea shelf and Canada Basin. Deep-Sea Res. Part II. dx.doi.org/10.1016/j.dsr2.2015.02.009

Brugel S., C. Nozais, M. Poulin, J-É Tremblay, L.A. Miller, K.G. Simpson, Y. Gratton, and S. Demers. 2009. Phytoplankton biomass and production in the southeastern Beaufort Sea in autumn 2002 and 2003. Mar Ecol Prog Ser. 377:63−77.

Cavalieri, D.J., C.L. Parkinson, P. Gloersen, and H. J. Zwally. 1996. Sea Ice Concentrations from Nimbus-7 SMMR and DMSP SSM/I-SSMIS Passive Microwave Data, Version 1.1, NASA National Snow and Ice Data Center Distributed Active Archive Center, doi:http://dx.doi.org/10.5067/8GQ8LZQVL0VL

Codispoti, L.A., C.N. Flagg, V. Kelly, and J.H. Swift. 2005. Hydrographic conditions during the 2002 SBI process experiments. Deep-Sea Res. Part II. 52: 3199–3226.

Codispoti, L.A., C.N. Flagg, V. Kelly, and J.H. Swift H. 2009. Hydrographic conditions during the 2004 SBI process experiments. Deep-Sea Res. Part II. 56: 1144–1163.

Cooper, L.W., T.E. Whitledge, J.M. Grebmeier, and T. Weingartner, T. 1997. The nutrient, salinity, and stable oxygen isotope composition of Bering and Chukchi Seas waters in and near Bering Strait. J. Geophys. Res. 102: 12563–12573.

Cota, G.F., L.R. Pomeroy, W.G. Harrison, E.P. Jones, F. Peters, W.M. Sheldon, and T.R. Weingartner. 1996. Nutrients, primary production and microbial heterotrophy in the southeastern Chukchi Sea: Arctic summer nutrient depletion and heterotrophy. Mar. Ecol. Prog. Ser. 135: 247–258.

Coupel, P., A. Matsuoka, D. Ruiz-Pino, M. Gosselin, D. Marie, J-É Tremblay, and M. Babin. 2015. Pigment Signatures of phytoplankton communities in the Beaufort Sea. Biogeosciences. 12: 991-1008. doi:10.5194/bg-12-991-2015.

Danielson, S.A., L. Eisner, C. Ladd, C. Mordy, L. Sousa, and T.J. Weingartner. 2017. A comparison between late summer 2012 and 2013 water masses, macronutrients, and phytoplankton standing crops in the northern Bering and Chukchi Seas. Deep-Sea Res. Part II. 135: 7–26.doi: 10.1146/annurev.genet.42.110807.091452

Eberhard, S., G. Finazzi, and F-Á. Wollman. 2008. The dynamics of photosynthesis. Annu. Rev. Genet. 42:463–515

Falkowski, P.G. and T.G. Owens. 1980. Light–shade adaptation: two strategies in marine phytoplankton, Plant Physiol. 66: 592-595.

Falkowski P.G., T.G. Owens, A.C Ley, and D.C Mauzerall.1981. Effect of growth irradiance levels on the ratio of reaction centers in two species of marine phytoplankton. Plant Physiol 68: 969–973.

Falkowski, P.G., Z. Dubinksy, and K. Wyman. 1985. Growth-irradiance relationships in phytoplankton. Limnol. Oceanogr. 30: 311-321.

Falkowski, P.G. and J.A. Raven. 2007. Aquatic photosynthesis, 2nd ed. Princeton Univ. Press.

Fortier M, L. Fortier , C. Michel, and L. Legendre. 2002. Climatic and biological forcing of the vertical flux of biogenic particles under seasonal Arctic sea ice. Mar Ecol Prog Ser 225: 1–16. doi:10.3354/meps225001

Frey, K.E., D.K Perovich, and B. Light. 2011. The spatial distribution of solar radiation under a melting Arctic sea ice cover. Geophys. Res. Lett. 38, doi:10.1029/2011GL049421

Galindo, V. and others. 2014. Biological and Physical Processes Influencing Sea Ice, Under-Ice Algae, and Dimethylsulfoniopropionate during Spring in the Canadian Arctic Archipelago. J Geophys Res-Oceans. 119: 3746–66. doi:10.1002/2013JC009497

Geider, R.J., J. LaRoche, R.M. Greene, and M. Olaizola. 1993. Response of the photosynthetic apparatus of *Phaeodactylum tricornutum* (*Bacillariophyceae*) to nitrate, phosphate, or iron starvation. J. Phycol. 29:755–66.

Geider, R.J., H.L. MacIntyre, and T.M. Kana. 1998. A dynamic regulatory model of phytolanktonic acclimation to light, nutrients, and temperature. Limnol. Oceanogr. 43: 679-694.

Gervais, F., U. Riebesell, and M.Y. Gorbunov. 2002. Changes in primary productivity and chlorophyll *a* in response to iron fertilization in the southern Polar Front Zone. Limnol. Oceanogr. 47: 1324-1335.

Gradinger, R. 2009. Sea ice algae: Major contributors to primary production and algal biomass in the Chukchi and Beaufort Seas during May/June 2002. Deep-Sea Res. II. 56: 1201-1212, doi:10.1016/j.dsr2.2008.10.016.

Gregg, W.W., and K.L. Carder. 1990. A simple spectral solar irradiance model for cloudless maritime atmospheres. Limnol. Oceanogr. 35: 1657-1675.

Grenfell, T.C. and G.A. Maykut. 1977. The optical properties of ice and snow in the Arctic basin. Journal of Glaciology. 18: 445-463.

Gruber, N. 2008. "The marine nitrogen cycle: overview and challenges." Nitrogen in the marine environment. Elsevier. ISBN: 978-0-12-372522-6.

Hansell, D.A., T.E. Whitledge, and J.J. Goering. 1993. Patterns of nitrate utilization and new production over the Bering-Chukchi Self. Cont. Shelf. Res. 13: 601-527.

Hameedi, M.J. 1978. Aspects of water column primary productivity in the Chukchi Sea during summer. Mar. Biol. 48: 37–48, doi:10.1007/BF00390529

Hill, V. and G. Cota. 2005. Spatial patterns of primary production on the shelf, slope and basin of the Western Arctic in 2002. Deep-Sea Res. Part II 52: 3344–3354. doi:10.1016/j.dsr2.2005.10.001

Hill, V., G.F. Cota, and D. Stockwell. 2005. Spring and summer phytoplankton communities in

the Chukchi and Eastern Beaufort Seas. Deep-Sea Res. II. 52:3369–3385, doi:10.1016/j.dsr2.2005.10.010

Holm-Hansen, O., C.J. Lorenzen, R.W. Holmes, and J.D.H. Strickland. 1965. Fluorometric Determination of Chlorophyll. ICES J Mar Sci. 30: 3-15, doi:10.1093/icesjms/30.1.3

Hsiao, S.I.C., M.G. Foy, and D.W. Kittle. 1977. Standing stock, community structure, species composition, distribution, and primary production of natural populations of phytoplankton in the southern Beaufort Sea. Can J Bot. 55: 685−694.

IPCC, 2014: Climate Change 2014: Synthesis Report. Contribution of Working Groups I, II and III to the Fifth Assessment Report of the Intergovernmental Panel on Climate Change [Core Writing Team, R.K. Pachauri and L.A. Meyer (eds.)]. IPCC, Geneva, Switzerland.

Karp-Boss L., and E. Boss. 2016. The Elongated, the Squat and the Spherical: Selective Pressures for Phytoplankton Shape. In: Glibert P., Kana T. (eds) Aquatic Microbial Ecology and Biogeochemistry: A Dual Perspective. Springer.

Kiefer, D.A. 1973. Chlorophyll *a* fluorescence in marine centric diatoms: Responses of chloroplasts to light and nutrient stress. Marine Bio. 23: 39-46.

Kiefer, D.A and B.G. Mitchell. 1983. A simple, steady state description of phytoplankton growth based on absorption cross section and quantum efficiency. Limnol. Oceanogr.28: 770-776.

Kolber, Z. S., O. Prasil, and P.G. Falkowski. 1998a. Measurements of variable chlorophyll fluorescence using fast repetition rate techniques: defining methodology and experimental protocols. Biochim. Biophys. Acta Bioenergetics.1367: 88-106.

Kolber Z., Zehr J., and P. Falkowski. 1988b. Effects of growth irradiance and nitrogen limitation on photosynthetic energy conversion in photosystem 11. Plant Physiol 88: 923-929.

Kropuenske, L. R., M. M. Mills, G. L. van Dijken, S. Bailey, D. H. Robinson, N. A. Welschmeyer, and K. R. Arrigo. 2009. Photophysiology in two major Southern Ocean phytoplankton taxa: Photoprotection in *Phaeocystis antarctica* and *Fragilariopsis cylindrus*. Limnol. Oceanogr. 54: 1176–1196, doi:10.4319/lo.2009.54.4.1176

Lavaud, J. 2007. Fast Regulation of Photosynthesis in Diatoms: Mechanisms, Evolution and Ecophysiology. Functional Plant Science and Biotechonology. 1:.267-287.

Laney, S.R. and H.M. Sosik. 2014. Phytoplankton assemblage structure in and around a massive under-ice bloom in the Chukchi Sea. Deep-Sea Res. Part II. 105: 30-41, doi: http://dx.doi.org/10.1016/j.dsr2.2014.03.012.

Laney, S.R., R.A. Krishfield, and J.M. Toole. 2017. The euphotic zone under Arctic Ocean sea ice: Vertical extents and seasonal trends. Limnol. Oceanogr. 62: 1910-1934. doi.org/10.1002/lno.10543

Lewis, M. R. and J. C. Smith. 1983. A Small Volume, Short- Incubation-Time Method for Measurement of Photosynthesis as a Function of Incident Irradiance. Mar. Ecol. Prog. Ser. 13: 99–102, doi:10.3354/meps013099.

Leu, E. S. Falk-Petersen, and D.O. Hessen. 2007. Ultraviolet radiation negatively affects growth but not food quality of arctic diatoms. Limnol. Oceanogr. 52: 787-797.

Litchman, E., P.J. Neale, and A.T. Banaszak. 2002. Increased sensitivity to ultraviolet radiation

in nitrogen-limited dinoflagellates: Photoprotection and repair. Limnol. Oceanogr. 47:86–94.

Lovejoy C., L. Legendre, M.J. Martineau, J. Bâcle, and C.H. von Quillfeldt. 2002. Distribution of phytoplankton and other protists in the North Water. Deep-Sea Res II. 49: 5027−5047.

Lowry, K.E., R.S. Pickart, M.M. Mills, Z.W. Brown, G.L. van Dijken, N.R. Bates, and K.R. Arrigo. 2015. The influence of winter water on phytoplankton blooms in the Chukchi Sea. Deep-Sea Res. Part II. 118: 53–72.

Lowry, K.E. and others. 2018. Under-ice phytoplankton bloom dynamics controlled by spring convective mixing in refreezing leads of open water. J. Geophys. Res. 123, doi.org/10.1002/2016JC012575.

MacIntyre, H.L., T.D. Kana, T. Anning, and R.J. Geider. 2002. Photoacclimation of photosynthesis irradiance response curves and photosynthetic pigments in microalgae and cyanobacteria. J. Phycol. 38: 17-38.

Maslanik, J.A., C. Fowler, J. Stroeve, S. Drobot, J. Zwally, D. Yi, and W. Emery. 2007. A younger, thinner Arctic ice cover: Increased potential for rapid, extensive sea ice loss. Geophys. Res. Lett. 34: L24501, doi:10.1029/2007GL032043

Matrai, P.A., E. Olson, S. Suttles, V. Hill, L.A. Codispoti, B. Light, and M. Steele. 2013. Synthesis of primary production in the Arctic Ocean: I. Surface waters, 1954-2007. Prog. Oceanog. 110: 93-106.

Matsuoka, A., V. Hill, Y. Huot, M. Babin, and A. Bricaud. 2011. Seasonal variability in the light absorption properties of western Arctic waters: Parameterization of the individual

components of absorption for ocean color applications. J. Geophys. Res. 116. doi:10.1029/2009JC005594.

McMinn, A. and E.N. Hegseth. 2004. Quantum yield and photosynthetic parameters of marine microalgae from the southern Arctic Ocean, Svalbard. J. Mar. Biol. Assoc. U. K. 84: 865-871.

Mitchell, B.G., M. Kahru, J. Wieland, and M. Stramska. 2002. Determination of spectral absorption coefficients of particles, dissolved material and phytoplankton for discrete water samples, p. 39–64. In J. L. Mueller, G. S. Fargion, and C. R. McClain (eds.), Ocean optics protocols for satellite ocean color sensor validation, Rev. 4, Vol. IV, NASA Tech. Memo. NASA/TM-2003-211621/Rev4-Vol.IV.

Moore, C.M. and others. 2003. Physical controls on phytoplankton physiology and production at a shelf sea front: a fast repetition-rate fluorometer based field study. Mar. Ecol. Prog. Ser. 259: 29-514.

Moore, C.M. and others. 2006. Phytoplankton photoacclimation and photoadaptation in response to environmental gradients in a shelf sea. Limnol. Oceanogr. 51: 936-939. doi: 10.4319/lo.2006.51.2.0936

Morel, A. and A. Bricaud. 1981. Theoretical results concerning light absorption in a discrete medium and application to specific absorption of phytoplankton. Deep-Sea Res. 28: 1375-1981.

Mundy, C. J., D. G. Barber, and C. Michel. 2005. Variability of snow and ice thermal, physical

and optical properties pertinent to sea ice algae biomass during spring. J. Mar. Syst. 58: 107–120.

Neukermans, G., R.A. Reynolds, and D. Stramski. 2014. Contrasting inherent optical properties and particle characteristics between an under-ice phytoplankton bloom and open water in the Chukchi Sea. Deep Sea Res II. 105: 59-73. dx.doi.org/10.1016/j.dsr2.2014.03.014.

Nymark, M. and others. 2009. An integrated analysis of molecular acclimation to high light in the marine diatom *Phaeodactylum tricornutum*. PloS ONE. 11:1-14. doi.org/10.1371/journal.pone.0007743

Olaizola, M., J. La Roche, Z. Kolber, and P.G. Falkowski. 1994. Non-photochemical quenching and the diadinoxanthin cycle in a marine diatom. Photosynth. Res. 41: 357–370.

Palmer, M.A. and others. 2011. Spatial and temporal variation of photosynthetic parameters in natural phytoplankton assemblages in the Beaufort Sea, Canadian Arctic. Polar Biol. 34: 1915–1928, doi:10.1007/s00300-011-1050-x

Palmer, M.A. and others. 2013. Light and nutrient control of photosynthesis in natural phytoplankton populations from the Chukchi and Beaufort seas, Arctic Ocean. Limnol. Oceanogr. 58: 2185–2205. doi: 10.4319/lo.2013.58.6.2185

Pavlov, A., T. Taskjelle, H.M. Kauko, B. Hamre, S.R. Hudson, P. Assmy, P. Duarte, M. Fernández-Méndez, C.J. Mundy, and M.A. Granskog. 2017. Altered inherent optical properties and estimates of the underwater light field during an Arctic under-ice bloom of *Phaeocystis pouchetii*. J. Geophys. Res.122: 4939-4961. doi:10.1002/2016JC012471.

Perovich, D.K., C.S. Roesler and W.S. Pegau. 1998. Variability in Arctic sea ice optical properties. J. Geophys. Res. 103: 1193-1208.

Perovich, D. and C. Polashenski. 2012. Albedo evolution of seasonal Arctic sea ice. Geophys. Res. Lett. 39: L08501. doi:10.1029/ 2012GL051432

Perrette, M., A. Yool, G.D. Quartly, E.E Popova. 2011. Near-ubiquity of ice-edge blooms in the Arctic. Biogeoscience 8, 515–524.

Pickart, R.S., G.W.K. Moore, C. Mao, F. Bahr, C. Nobre, and T. J. Weingartner. 2016. Circulation of winter water on the Chukchi shelf in early Summer, Deep-Sea Res. II, 130(C), 56–75, doi:10.1016/j.dsr2.2016.05.001

Platt, T., C.L. Gallegos, and W.G. Harrison. 1980. Photoinhibition of photosynthesis in natural assemblages of marine phytoplankton. J. Mar. Res. 38: 687–701.

Popova, E.E. and others. 2012. What controls primary production in the Arctic Ocean? Results from an intercomparison of five general circulation models with biogeochemistry. J. Geophys. Res. Oceans. 117, doi:10.1029/2011JC007112.

Ras, J., H. Claustre, and A.C. Uitz. 2008. Spatial variability of phytoplankton pigment distributions in the Subtropical South Pacific Ocean: comparison between in situ and predicted data. Biogeosciences. 5(2): 353-369.

Röttgers, R. and S. Gehnke. 2012. Measurement of light absorption by aquatic particles: improvement of the quantitative filter technique by use of an integrating sphere approach. Appl. Optics, 51, 1336–1351.

Sakshaug, E. 2004. Primary and secondary production in the Arctic seas. In: Stein, R., Macdonald, R.W. (Eds.), The Organic Carbon Cycle in the Arctic Ocean. Springer, New York, pp. 57–81.

Selz, V. and others. 2017. Ice algal communities in the Chukchi and Beaufort Seas in spring and early summer: composition, distributions, and coupling with phytoplankton assemblages. Limnol. Oceanogr., doi.org/10.1002/lno.10757

Soohoo, J. B., A.C. Palmisano, S.T. Kottmeier, M. P. Lizotte, S. L. Soohoo, AND C. W. Sullivan. 1987. Spectral light absorption and quantum yield of photosynthesis in sea ice microalgae and a bloom of *Phaeocystis pouchetii* from McMurdo Sound, Antarctica. Mar. Ecol. Prog. Ser. 39: 175–89, doi:10.3354/meps039175

Strass, V. H. and E.M. Nöthig. 1996. Seasonal shifts in ice edge phytoplankton blooms in the Barents Sea related to the water column stability. Polar Biol. 16: 409−422.

Stolte, W. and R. Riegman. 1995. Effect of phytoplankton cell size on transient-state nitrate and ammonium uptake kinetics. Microbiology. 141: 1221-1229.

Stroeve, J. C., T. Markus, L. Boivert, J. Miller, and A. Barrett. 2014. Changes in Arctic Melt Season and Implications for Sea Ice Loss. Geophys Res Lett. 41: 1216–1225. doi:10.1002/2013GL058951.

Sugget, D.J., C.M. Moore, A.E. Hickman, and R.J. Geider. 2009. Interpretation of fast rate repetition (FRR) fluorescence: signatures of phytoplankton community structure versus physiological state. Mar. Ecol. Prog. Ser. 376: 1-19.

Suggett, D. J., O. Prášil, and M.A. Borowitzka. 2010. Chlorophyll *a* fluorescence in aquatic sciences: methods and applications. Springer. doi: 10.1007/978-90-481-9268-7 .

Suzuki, K. and others. 2002. East–west gradients in the photosynthetic potential of phytoplankton and iron concentration in the subarctic Pacific Ocean during early summer. Limnol. Oceanogr. 47: 1581-1594.

Tambi, H., A. Fonnes Flaten, J. K. Egge, G. Bødtker, A. Jacobsen, and T.F. Thingstad. 2009. Relationship between phosphate affinities and cell size and shape in various bacteria and phytoplankton. Aquat. Microb. Ecol. 57: 311-320. doi: 10.3354/ame01369.

Tassan, S. and G.M. Ferrari. 1995. An alternative approach to absorption measurements of aquatic particles retained on filters. Limnol. Oceanogr. 40: 1358–1368.

Tassan, S. and G.M. Ferrari. 2002. A sensitivity analysis of the "Transmitance-Reflectance" method for measuring high absorption by aquatic particles. J. Phyto. Res. 24: 757–774.

Tremblay J-É., C. Michel, K.A. Hobson, M. Gosselin, and N.M. Price. 2006. Bloom dynamics in early opening waters of the Arctic Ocean. Limnol. Oceanogr. 51: 900-912.

Tremblay J-É. and J. Gagnon. 2009. The effects of irradiance and nutrient supply on the productivity of Arctic waters: a perspective on climate change. In: Nihoul J.C.J., Kostianoy A.G. (eds) Influence of Climate Change on the Changing Arctic and Sub-Arctic Conditions. NATO Science for Peace and Security Series C: Environmental Security. Springer, Dordrecht. 73-93.

Trimborn, S., S. Thoms, K. Petrou, S. Kranz, and B. Rost. 2013. Photophysiological responses of Southern Ocean phytoplankton to changes in CO_2 concentrations: Short-term versus acclimation effects. J. Exp. Biol. 451: 44-54. doi: dx.doi.org/10.1016/j.jembe.2013.11.001

van der Poll, W.H., M.A. van Leeuwe, J. Roggeveld, and A.G.J. Buma. 2005. Nutrient limitation and high irradiance acclimation reduce PAR and UV-induced viability loss in the Antarctic diatom *Chaetoceros Brevis* (*Bacillariophycae*). J. Phycol. 41: 840-850. doi: 10.1111/j.1529-8817.2005.00105.x

Van Leeuwe, M.A., B. van Sikkelerus, W.W.C. Gieskes, and J. Stefels, J. 2005. Taxon-specific differences in photoacclimation to fluctuating irradiance in an Antarctic diatom and a green flagellate. Mar. Ecol. Prog. Ser. 288, 9-19.

Varela, D.E., D.W. Crawford, I.A. Wrohan, S.N. Wyatt, and E.C. Carmack. 2013. Pelagic primary productivity and upper ocean nutrient dynamics across Subarctic and Arctic Seas, J. Geophys. Res. Oceans. 118: 7132–7152, doi:10.1002/2013JC009211

Walsh, J.J. and others. 2005. A numerical model of seasonal primary production within the Chukchi/Beaufort Seas. Deep-Sea Research II. doi:10.1016/j.dsr2.2005.09.009

Zapata, M., F. Rodriguez, and J.L. Garrido. 2000. Separation of Chlorophylls and Carotenoids from Marine Phytoplankton: A New HPLC Method Using a Reversed Phase C8 Column and Pyridine-Containing Mobile Phases. Mar Ecol Prog Ser. 195: 29-45. doi:10.3354/meps195029

ACKNOWLEDGEMENTS

This research is a contribution to the ICESCAPE project (NASA Ocean Biology and Biogeochemistry, Cryosphere Science NNX10AF42G) and SUBICE project (NSF Division of Polar Programs PLR-1304563). This work is also supported by NASA Earth and Space Science Fellowship grant NNX16AO08H awarded to K.M. Lewis. We thank the entire ICESCAPE and SUBICE teams including Dr. Sam Laney (Woods Hole Oceanographic) for collecting and processing ICESCAPE IFCB images, Jan Nash-Arrigo for her SUBICE sampling and educational outreach, Caroline Ferguson and Erin Dillon (Stanford University) for sampling during SUBICE, and Joannie Ferland (Université Laval) for assisting in P-E measurements during SUBICE. We also thank the USCGC Healy ICESCAPE and SUBICE crew for their operations and support.

FIGURE LEGENDS

Figure 1. Subset of stations from SUBICE that qualify as low-light, high-nutrients (LLHN; green) and from ICESCAPE 2010 and 2011 that qualify as high-light, low-nutrients (HLLN; yellow) overlain on bathymetry (grey).

Figure 2. Average incoming daily photosynthetically active radiation (PAR; µEin m^{-2} s^{-1}) during the sampling period of each field expedition modeled using the Gregg & Carder (1990) radiative transfer model.

Figure 3. Mean photosynthesis-irradiance (P-E) curves in bold measured for low-light, high-nutrients (LLHN; green) and high-light, low-nutrients (HLLN; yellow) conditions (Table 4). Thin lines of the same color represent the upper and lower limit of error based on the standard deviation at each light level. Gray line denotes the mean photoacclimation parameter (E_k) for both seasons (~67 µEin m^2 s^{-1}) (Table 4). Mean surface PAR at solar noon is represented by dashed line for LLHN (green) and HLLN (yellow) (Table 2). Mean photosynthetic rates based on mean surface PAR at solar noon (~0.6 mg C mg^{-1} Chl *a* h^{-1} for both seasons) is represented by the dots outlined in black on each P-E curve.

Table 1. Mean daily surface nitrate (NO_3^-) measurements for stations categorized as low-light, high-nutrients (LLHN) and high-light, low-nutrients (HLLN).

	Date	NO_3^- (µM)
LLHN	5/23/14	14.69
	5/24/14	15.32
	5/25/14	12.21
	5/26/14	13.08
	5/27/14	11.36
	5/28/14	14.44
	5/29/14	12.18
	5/30/14	10.36
	5/31/14	9.02
	6/1/14	10.3
	6/2/14	10.77
	6/5/14	15.18
	6/6/14	15.83
	6/7/14	13.5
	6/10/14	14.01
	6/11/14	12.22
	6/12/14	14.84
	6/13/14	17.44
	6/14/14	16.05
	6/15/14	15.48
	6/16/14	16.55
	6/17/14	16.14
	6/18/14	16.86
	6/19/14	15.97
	LLHN mean 13.91 ± 2.37	
HLLN	6/18/10	0.05
	6/20/10	< 0.02
	6/21/10	< 0.02
	6/22/10	0.21
	6/23/10	< 0.02
	6/24/10	0.11
	6/30/10	0.17
	7/1/10	< 0.02
	7/5/10	< 0.02
	7/7/10	0.46
	7/8/10	0.04
	7/9/10	< 0.02
	7/15/10	< 0.02
	7/16/10	< 0.02
	6/28/11	0.04
	6/29/11	< 0.02
	6/30/11	< 0.02
	7/1/11	< 0.02
	7/2/11	0.09
	7/3/11	< 0.02
	7/4/11	< 0.02
	7/8/11	< 0.02
	7/9/11	< 0.02
	7/10/11	< 0.02
	7/15/11	< 0.02
	7/16/11	< 0.02
	7/21/11	< 0.02
	7/22/11	< 0.02
	7/23/11	0.09
	7/24/11	0.04
	HLLN mean 0.05 ± 0.09	

Table 2. Surface photosynthetically active radiation (PAR; µEin m^{-2} s^{-1}) measured at solar noon beneath the ice at low-light, high-nutrients (LLHN) stations and in open water for high-light, low-nutrients (HLLN) stations.

	Date	PAR mean	PAR std dev
LLHN	5/24/14	0.8	0.8
	5/28/14	4.1	4.4
	6/2/14	2.9	2.9
	6/5/14	7.4	4.3
	6/6/14	3.4	1.5
	6/11/14	14.3	20.2
	6/13/14	7.3	5.4
	6/15/14	38.3	19.7
	6/17/14	52.0	18.5
LLHN average 14.5 ± 18.1			
HLLN	6/18/10	1020.4	24.6
	6/20/10	1357.7	8.2
	6/21/10	974.1	359.8
	6/23/10	1191.2	70.4
	6/24/10	1184.6	16.3
	6/30/10	798.5	21.3
	7/1/10	705.1	476.2
	7/5/10	882.9	350.9
	7/7/10	878.6	272.2
	7/9/10	1044.2	170.4
	7/15/10	441.0	6.2
	7/16/10	116.4	4.2
	6/28/11	305.4	102.2
	6/29/11	629.0	284.6
	6/30/11	451.4	221.0
	7/1/11	831.7	92.0
	7/2/11	456.0	87.8
	7/3/11	417.5	114.1
	7/8/11	990.8	193.5
	7/9/11	764.8	354.5
	7/15/11	630.4	322.7
	7/16/11	936.9	364.5
	7/21/11	718.8	43.4
	7/22/11	658.0	59.8
	7/23/11	683.1	100.7
HLLN average 762.7 ± 143.6			

Table 3. Seasonal classifications of the surface ocean environment based on NO_3^- and sea ice concentration. Only low-light, high-nutrients (LLHN) and high-light, low-nutrients (HLLN) provided enough samples to be used in statistical analyses.

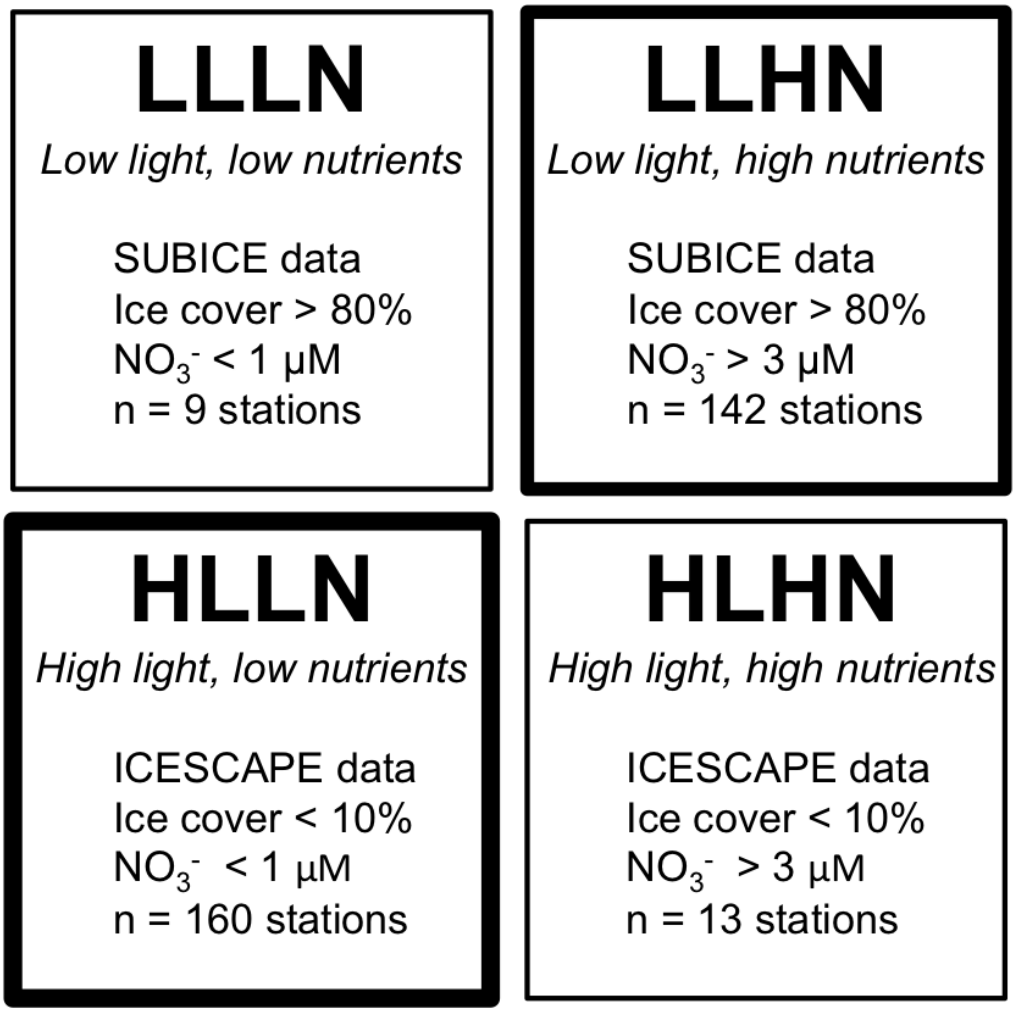

Table 4. Seasonal means of photosynthetic parameters for surface phytoplankton measured during pre-bloom low-light, high-nutrients (LLHN) and post-bloom high-light, low-nutrients (HLLN) conditions. Parameters showing significant changes ($p < 0.01$) are illustrated by grey background. Abbreviations and units: Chlorophyll *a* (Chl *a*) = mg m^{-3}; spectrally averaged Chl *a*-specific absorption ($\bar{a}^*$) = m^2 mg^{-1} Chl *a*; Chl *a*-specific absorption of blue to red peaks (a^*_{ph} blue/red) = dimensionless; particulate organic carbon (POC), photoprotective pigments (PPP), and photosynthetic pigments (PSP) normalized by Chl *a* = g:g; maximum photochemical efficiency of photosystem II ($F_v:F_m$) = dimensionless; turnover time (τ_{PSII}) = ms; functional absorption cross-section (σ_{PSII}) = $Å^2$ $quanta^{-1}$; maximum photosynthetic rate (P^*_{max}) = mg C mg Chl a^{-1} h^{-1}, photosynthetic efficiency (α^*) and photoinhibition (β^*) = mg C mg Chl a^{-1} h^{-1} (µEin m^{-2} s^{-1})$^{-1}$; photoacclimation parameter (E_k) = µEin m^{-2} s^{-1}, quantum yield (Φ_m) = mol C (mol quanta absorbed)$^{-1}$; maximum and average growth rate (u_{max} and u_{avg}) = d^{-1}; primary production (PP) = g C m^{-2} d^{-1}.

	LLHN mean	LLHN sd	LLHN n	HLLN mean	HLLN sd	HLLN n	t-statistic	p-value
Chl *a*	**1.71**	1.96	512	**1.53**	4.44	208	-0.533	0.594
$\bar{a}^*$	**0.014**	0.019	175	**0.029**	0.023	50	4.09	0.000
a^*_{ph} blue : red	**2.02**	0.65	164	**2.69**	0.69	104	7.98	0.000
POC / Chl*a*	**119**	120	219	**314**	170	107	10.6	0.000
PPP / Chl*a*	**0.074**	0.017	43	**0.153**	0.065	81	10.2	0.000
PSP / Chl*a*	**0.482**	0.046	43	**0.320**	0.089	81	-13.4	0.000
$F_v:F_m$	**0.43**	0.13	243	**0.39**	0.11	21	-1.54	0.136
τ_{PSII}	**1.01**	0.23	243	**0.79**	0.34	21	-2.86	0.009
σ_{PSII}	**497**	83.5	243	**379**	101	21	-5.24	0.000
P^*_{max}	**2.42**	0.92	40	**0.83**	0.45	82	-4.5	0.000
α^*	**0.043**	0.031	40	**0.017**	0.016	82	-5.02	0.000
E_k	**67.8**	63.2	40	**68.5**	42.6	82	0.064	0.949
β^*	**0.014**	0.024	40	**0.0006**	0.0005	10	-3.4	0.002
Φ_m	**0.163**	0.089	34	**0.020**	0.025	34	-8.95	0.000
μ_{max}	**1.31**	0.50	37	**0.09**	0.12	78	-14.7	0.000
μ_{avg}	**0.27**	0.12	37	**0.07**	0.09	10	-5.99	0.000
PP	**1.05**	0.99	21	**2.5**	4.6	23	1.97	0.056